ARTICLE

Surface-Potential-Regulated Transmembrane and Cytotoxicity of Chitosan/Gold Hybrid Nanospheres

Yin Ding,[†] Xiaochen Bian,[‡] Wei Yao,[†] Rutian Li,[§] Dan Ding,[†] Yong Hu,[||] Xiqun Jiang,*[,†] and Yiqiao Hu[‡]

Laboratory of Mesoscopic Chemistry and Department of Polymer Science and Engineering, College of Chemistry & Chemical Engineering, Nanjing University, Nanjing 210093, P.R. China, Department of Biochemistry, College of Life Science, Nanjing University, Nanjing 210093, P. R. China, Department of Oncology, Drum Tower Hospital Affiliated to Nanjing Medical University & Clinical Cancer Institute of Nanjing University, Nanjing 210008, P. R. China, and National Laboratory of Solid State Microstructure, Department of Material Science and Engineering, Nanjing University, Nanjing 210093, P. R. China

ABSTRACT Chitosan−gold hybrid nanospheres with varying surface zeta potentials were designed as a model system to investigate cell internalization. Gold nanoparticle was selected as optical marker to facilitate the visualization of the hybrid polymeric nanosphere internalization course and the localization in the cell by dark-field optical microscopy and transmission electron microscopy. It is found that surface potential has significant biological implications in the transmembrane efficiency, intracellular fate, and cytotoxicity of the hybrid nanospheres. Compared to those with lower surface potential, the spheres with higher surface potential show a faster cell uptake and enhance the nucleus targeting. However, too high a surface potential may destabilize the cell membrane and induce cell damage as well as cytotoxicity. These finding can help us to design suitable drug or gene nanocarriers with low cytotoxicity and high delivering ability.

KEYWORDS: chitosan • cell uptake • cytotoxicity • transmembrane ability

INTRODUCTION

Polymeric nanospheres, especially biocompatible ones, are of great interest in biomedicine as cargos to deliver imaging agents (1−3), phototherapy agents (4, 5), and drugs (6, 7) into the target cells. However, controlling the balance between effectively crossing the cell membrane to reach intracellular target compartments and inducing toxic effects for these nanospheres is one of the key challenges in these fields (8, 9). Several studies have suggested that physicochemical properties of nanocarriers, such as size, surface zeta potential, and shape of particles, are important parameters in designing suitable cell tracking and drug-carrier nanoparticulate systems (10−12) because they determine the mechanism and rate of cell uptake of a nanoparticle and its ability to permeate through tissue. For example, Chan et al. have found that cellular uptake of gold nanoparticles was related to size and shape, and the particles with a size of 50 nm had highest uptake efficiency (10b). On the other hand, nanoparticle surface charge also has a prominent effect on endocytosis, intracellular pathway, and cell response to the nanoparticles. Cationic nanoparticles have shown approximate 2-folds greater uptake than anionic ones in HeLa cells (13). Recent work has shown that the type of surface charge seems to be a more important factor in determining the transmembrane crossing ability by cancer cells, and positively charged gold nanoparticles are internalized more easily by the SK-BR-3 cells than other types of gold nanoparticles (14). Therefore, understanding the role of surface charges in cellular adsorption and internalization is of primary importance in the development and optimization of polymeric drug carriers. However, up to now, previous investigations on surface charge effects on cell uptake did not include careful control of the size of polymer nanoparticles. Thus, the reported surface charge effect is not clear in physicochemical terms.

On the other hand, visualization of polymeric nanoparticles in cell is of great importance to evaluate and optimize the carriers (15). Spatial and temporal tracking of polymer nanoparticles in cells still remain challenging. Although fluorescently labeled nanoparticles can provide a rapid, simple, and sensitive means to quantify cell-associated nanoparticles by fluorometry (16), the leakage of the fluorescent molecules from the nanoparticles, photobleaching of fluorophores, and disturbance of tissue fluorescence are unavoidable. As an alternative, gold nanoparticles offer enough contrast for imaging with optical microscopes due to their strong plasmon enhanced absorption and high light-scattering ability (17, 18), which can provide detailed infor-

* To whom correspondence should be addressed. Fax: +86 25 83317761. E-mail: jiangx@nju.edu.cn.

Received for review February 4, 2010 and accepted April 16, 2010

[†] College of Chemistry & Chemical Engineering, Nanjing University.
[‡] College of Life Science, Nanjing University.
[§] Nanjing Medical University & Clinical Cancer Institute of Nanjing University.
[||] Department of Material Science and Engineering, Nanjing University.

DOI: 10.1021/am1001019

Published on Web 04/26/2010

mation on the intracellular location of gold particles by combining optical and electronic microscopies (10b, 19). Besides, the transmembrane crossing efficiency of gold particles can be easily measured by inductively coupled plasma mass spectroscopy (ICP-MS), which is capable of detecting Au ion concentration down to the parts perbillion level and is well-suited for the determination of the number of metal nanoparticles contained in cells (10b), whereas most of these studies about the cell uptake were performed with gold nanoparticles alone, which are far from the real polymer drug nanocarriers. Very recently, we found that the gold-associated hybrid polymeric hollow nanospheres not only could overcome the cellular barriers to lighten up the entire cell but also reveal the intracellular fate of polymer spheres by means of dark-field optical and electronic microscopies (20).

Here, we report the chitosan−gold hybrid nanospheres (CGHNs) with various surface zeta potentials to investigate the influence of surface potential of polymer nanocarriers on cell uptake and cytotoxicity. Gold nanoparticle encapsulated as an optical marker enables us easily visualize the internalization course and intracellular localization of polymer spheres by dark-field optical and electronic microscopies. Combing ICP-MS technique, gold content inside cells was quantitatively determined after the internalization of gold-associated polymeric spheres, which also provides the cell internalization situation of polymer spheres directly. Making full use of gold nanoparticles tagging, we found that the transmembrane crossing efficiency, intracellular fate and cytotoxicity of the polymer nanospheres were highly dependent on their surface zeta potential. The nanospheres with higher surface potential result in a faster cell uptake and enhance the cell nuclear targeting. However, too high a surface potential may destabilize the cell membrane and induce cell damage as well as cytotoxicity. These results would assist us in the future to design polymer nanocarriers for drug and gene delivery systems.

EXPERIMENTAL SECTION

Materials. Water-soluble chitosan (WCS) with a number average molecular weight (M_n) of 5000 Da was purchased from Yuhuan Biomedical Company (Zhejiang, China) and used without further purification. Ethylene diamine tetraacetic acid (EDTA) (Sigma), glutaraldehyde (GA) (Sigma), 3-[4, 5-dimehyl-2-thiazolyl]-2, 5-diphenyl-2H-tetrazolium bromide (MTT) (Sigma), Triton X-100 (Sigma), and $HAuCl_4$ (Aldrich) were used as received. All other ingredients were analytical grade unless otherwise stated.

Preparation of WCS−EDTA Composite Nanospheres. Briefly, 50 mg of WCS were first dissolved in 10 mL of water. Ten milligrams of EDTA was then added to the WCS aqueous solution and stirred until dissolution. Ethanol was then added dropwise to the system under vigorous stirring, and the clear solution turned opalescent when the concentration of ethanol exceeded a critical value (about 30%), implying the formation of colloidal nanospheres. After that, 90, 180, and 270 μL of GA solution (2.5%) was added to the system, respectively, in order to cross-link the generated nanospheres at room temperature overnight. The cross-linked nanospheres were purified using centrifugation, followed by redispersing the sediment into ethanol aqueous solution (40% v/v).

Preparation of Chitosan−Gold Hybrid Nanospheres (CGHNs). The above suspension containing WCS-EDTA composite nanospheres with a concentration of 0.25% w/v was mixed with 0.02 M $HAuCl_4$ solution at 70 °C water bath under stirring for 10 min. It was then slowly cooled and dialyzed (cutoff = 12 kDa) against pure water for 24 h to remove the free EDTA molecules. Inductively coupled plasma mass spectroscopy (ICP-MS) and thermogravimetric analysis (TGA) results indicated that the actual gold-to-chitosan ratio (w/w) in the final hybrid nanospheres is 2.9%. All the samples are calculated in accordance with the concentration of chitosan.

Preparation of FITC-Labeled Chitosan−Gold Hybrid Nanospheres. FITC-labeled CGHNs were prepared as reported with some modifications (11e). Three milliliters of methanol with 2.0 mg/mL FITC solution was added into 50 mL of prepared CGHNs solution, and the mixture was stirred at room temperature for 24 h in the dark. These FITC-labeled CGHNs were then separated by centrifugation at 4 °C. The obtained sediment was washed and redispersed in the mixture of methanol and distilled water (1:9 v/v) three times to remove the unreacted FITC. Finally, the obtained FITC labeled CGNHs were dispersed in aqueous solution with a pH value of 5.0 for the cell experiment.

Characterization of CGHNs. TEM (JEOL TEM-100) was used to measure the microstructure of CGHNs by dropping a sample onto the nitrocellulose-covered copper grid at room temperature without staining. SEM (JEOL JSM-6700) was used to observe the surface morphology of the hybrid nanospheres. The samples were placed on silicon wafer and plated with Pt before being characterized. Brookhaven BI-9000AT instrument (Brookhaven Instruments Corporation) was used to measure the mean diameter and size distribution of CGHNs. Zeta potential of the nanospheres was obtained with a Zetaplus (Brookhaven Instruments Corporation, USA). Each sample was adjusted to a concentration of 0.05% (w/v) in filtered water and sonicated before measurement. All results were the average of triplicate measurements and the values reported are the mean value (SD).

In vitro Cytotoxicity of CGHNs. The in vitro cytotoxicity of CGHNs was determined by standard MTT assays, using human gastric carcinoma cell line BGC 823. Cells were seeded in a 96-well plate at a density of 5000 cells per well and incubated at 37 °C in a humidified atmosphere with 5% CO_2. The culture medium was RPMI 1640 medium supplemented with 10% calf blood serum and changed every day until 80% confluence was reached. The medium was then replaced with 200 μL medium containing CGHNs with different surface zeta potentials. One row of 96-well plates was used as control with 200 μL of culture medium only. After incubation for 44 h, 20 μL of 10 mg mL^{-1} MTT solution was added to each well and the plate was incubated for 4 h, allowing the viable cells to reduce the yellow MTT into dark blue formazan crystals, which were dissolved in 200 μL of dimethyl sulfoxide (DMSO). The absorbance of individual wells was measured at 570 nm by an ELISA reader (Huadong, DG-5031, Nanjing). Cell viability was determined by following equation:

$$\text{cell viability } \% = \text{Abs}_{\text{test}}/\text{Abs}_{\text{ref}} \times 100\%$$

Dark-Field Microscopy Measurement of Cells. BGC 823 cells were cultured onto 20 mm glass coverslips in a six-well plate in RPMI 1640 medium supplemented with 10% calf blood serum at 37 °C in a humidified atmosphere with 5% CO_2, and allowed to grow for 2 days. Then the medium was replaced with 2 mL medium containing CGHNs (0.4 mg/mL, chitosan-based) with different surface zeta potentials. After incubation for 4 h, the coverslip with cell monolayer was taken out from the medium, washed three times with ice-cold phosphate buffered saline (PBS) and fixed with fresh paraformaldehyde (PFA) 4%

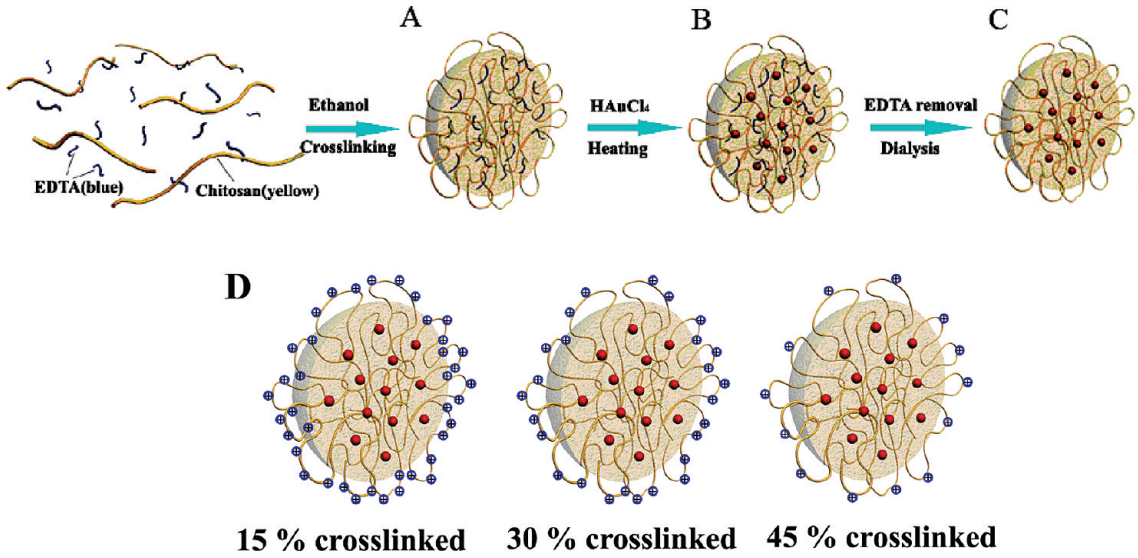

FIGURE 1. Schematic illustration of the preparation of CGHNs with different surface zeta potential by cross-linking different amount surface amino groups of chitosan. Au nanoparticles are shown as red dots.

(w/v). The light-scattering images were recorded by Olympus BX51 microscope with a dark-field condenser (U-DCW). Imaging was accomplished through collection of the scattered light using a 40 × objective, and dark-field pictures were taken using a Cannon digital camera. All images were compiled using Image-Pro Plus (IPP) software (MEDIA CYBERNETICS, USA). The images are representatives of the original data.

Laser Scanning Confocal Microscopy Measurement of Cells. BGC 823 cells were exposed to 0.4 mg/mL FITC-CGHNs (chitosan-based) for 4 h in a 6-well plate with a standard RPMI 1640 medium. These cells were then washed three times with PBS at 4 and 37 °C, successively. Next, the cells obtained were dehydrated and fixed by formaldehyde. The nuclei were then stained with Hoechst 33258 and these stained cells were observed using a confocal system (Zeiss LSM 710, Germany) by the green and blue channels.

Transmission Electron Microscopy Measurement of Cells. BGC 823 cells were exposed to 1.0 mg/mL CGHNs for 4 h in a 150 mL flask with standard RPMI 1640 medium. Those cells were then washed three times with PBS at 4 and 37 °C, respectively. After that, cells were detached from the flask by trypsin-EDTA and collected by centrifugation. The cells obtained were dehydrated, fixed by formaldehyde, and embedded in an epoxy resin. Sections approximately 50−70 nm thick were obtained by microtoming the resin sample at room temperature using Ultracut-E ultramicrotome instruments (Reichert-Jung, Leica Microsystems, Austria) for TEM measurement.

Measurement of Au Concentration in the Cells. BGC 823 cells were seeded at 1.0×10^4 cells/cm^2 onto 20 mm glass coverslips and were cocultured with CGHNs like for dark-field microscopy measurement. The cells were washed with ice-cold PBS three times and solubilized with 1 mL of 0.5% Triton X-100 in 0.2 M NaOH. Aqua regia was added to allow dissolution of the CGHNs. These clear acidic solutions were diluted for further testing. The mass of gold in CGHNs inside the BGC 823 cells was measured by detecting the gold concentration with ion-coupled plasma-mass spectrometry (ICP-MS, Hewlett-Packard 4500).

RESULTS AND DISCUSSION

Preparation of CGHNs. Chitosan−gold hybrid nanospheres (CGHNs) were prepared following a strategy as schematically illustrated in Figure 1, according to our previous work with some modifications (21). First, water-soluble and low-molecular-weight chitosan (WCS) and ethylene diamine tetraacetic acid (EDTA) composite nanospheres (WCS−EDTA) were prepared by adding ethanol, a nonsolvent for both chitosan and EDTA, into the aqueous solution consisting of WCS and EDTA to facilitate the counterion condensation between WCS and EDTA, resulting in WCS and EDTA to assembly into the colloidal nanospheres. Thus, the interior of WCS−EDTA composite nanospheres is mainly made of hydrophobic neutral polyelectrolyte−counterion complexes formed between WCS and EDTA, while the outer shell is the protonated and positive charged WCS chains. WCS−EDTA nanospheres with various surface zeta potentials were then generated by corsslinking different amount of amino groups in WCS-EDTA nanospheres with a predetermined amount of glutaraldehyde (GA) at room temperature (Figure 1A). WCS−EDTA nanospheres with about 15, 30, and 45% cross-linking degree of amino groups were obtained (determined by quantitation of the free primary amines remaining in the WCS using the well-characterized ninhydrin method) (22, 23), respectively. These WCS-EDTA nanospheres with different cross-linked degrees were mixed with allowed amount of Au salt feeding, respectively, and heated to 70 °C to convert Au salt in situ into gold nanoparticles in WCS−DTA nanospheres (Figure 1B, and the Supporting Information, Figure S1 and S2 as well as Table S1). At this stage, EDTA not only acts as a building block of the composite nanospheres but also a reductant in the system, whereas the good affinity of chitosan with gold salt and the potential stabilization effect offered by chitosan moieties for gold nanoparticles are also favorable factors in the preparation of chitosan−gold hybrid nanospheres through this approach. In addition, the payload of Au nanoparticles can be controlled by the addition amount of Au salt in the system. After the reduction, remaining EDTA inside the WCS-EDTA nanospheres was removed by dialysis against weak basic aqueous solution because of its small molecule character (Figure 1C). Thus, the pure chitosan−gold hybrid

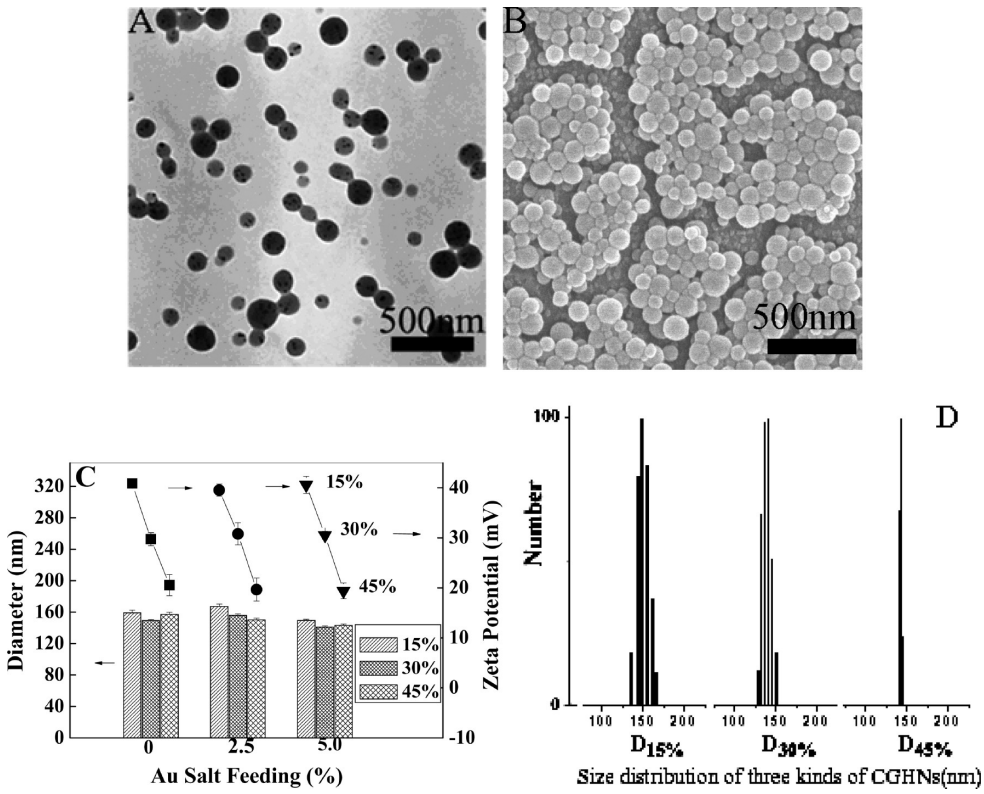

FIGURE 2. (A) TEM and (B) SEM images of CGHNs; (C) mean hydrodynamic diameters D_h and zeta potentials of CGHNs obtained by varying Au salt feeding and cross-linking degree of 15, 30, and 45%; (D) hydrodynamic diameter D_h distribution of the CGHNs with 5% Au salt feeding (Chitosan based) and cross-linking degree of 15, 30, and 45% in 1640 cell culture medium without serum.

nanospheres (CGHNs) with different surface zeta potentials were obtained (Figure 1D).

Surface Zeta Potential Effect on the Cell Internalization. Figure 2 shows the typical transmission electron microscopy (TEM) image (Figure 2A) and scanning electron microscopy (SEM) image (Figure 2B) of the CGHNs with 30% cross-linking degree after dialysis. It can be seen that the nanospheres have a spherical shape and smooth outline with about 120 nm size. The markedly higher electron density of gold enables the direct visualization of the existence of gold nanoparticles within the chitosan nanospheres (Figure 2A). The hydrodynamic diameters and zeta potentials of these obtained hybrid nanospheres with 15, 30, and 45% cross-linking degrees as a function of the amount of Au added are displayed in Figure 2C. It is clearly shown that whatever the amount of Au salt feeding or the sphere's cross-linking degree has almost no effect on the hydrodynamic diameters of the CGHNs, which is maintained around 140 nm, slightly larger than that measured by TEM because of their hydration state. However, the zeta potential is affected by the cross-linking degree. Higher cross-linking degree results in lower surface zeta potential. It is reasonable that the positive zeta potential of CGHNs is aroused from the protonated amino groups in the hybrids from chitosan molecules. The higher cross-linking degree leads to the decrease of the amount of protonated amino groups. Consequentially, the zeta potential of the nanospheres reduces. In addition, as the cell internalization marker, these hybrid nanospheres should be stable in the cell culture medium, and thus the particle size and the zeta potential of these CGHNs were also measured to evaluate their stability in the cell culture medium. Because of the good hydrophilicity of the chitosan used here, chitosan–gold hybrid nanosphere system puts up the superior dispersing stability and maintains narrow dispersed property in size even in RMPI 1640 cell culture medium (Figure 2D). Moreover, the nanospheres' surface zeta potential seems not to be affected by RMPI 1640 cell culture medium because the zeta potentials of the CGHNs did not change in 1640 cell culture medium (data not shown). On the basis of the above results, these CGHNs seem to be the suitable cell imaging agent to monitor the cell internalization and intracelullar fate of CS nanospheres.

To investigate the surface zeta potential effect on the cell internalization, we examined the uptake of 140-nanometer-sized CGHNs with different surface zeta potentials by BGC 823 cells by dark-field optical microscope utilizing the light scattering property of gold nanoparticle encapsulated in CS nanospheres. A semiquantitative analysis based on light scattering intensity was also performed to evaluate the difference in uptake among the three different surface zeta potential formulations, using Image-Pro Plus (IPP) software as described by Massa et al. (24). A series of CGHNs with the same size but varying surface zeta potentials (19.39, 30.51, and 40.60 mV) were incubated with BGC 823 cells at 37 °C for 4 h, respectively. Bright-field images (Figure 3A, C, E) show that all cells proliferate very well and maintain their normal configuration for all the CGHNs regardless of the surface zeta potential. In the corresponding dark-field images (Figure 3B, D, F), it is clearly shown that CGHNs with different zeta potentials, such as 19.39, 30.51, and 40.60

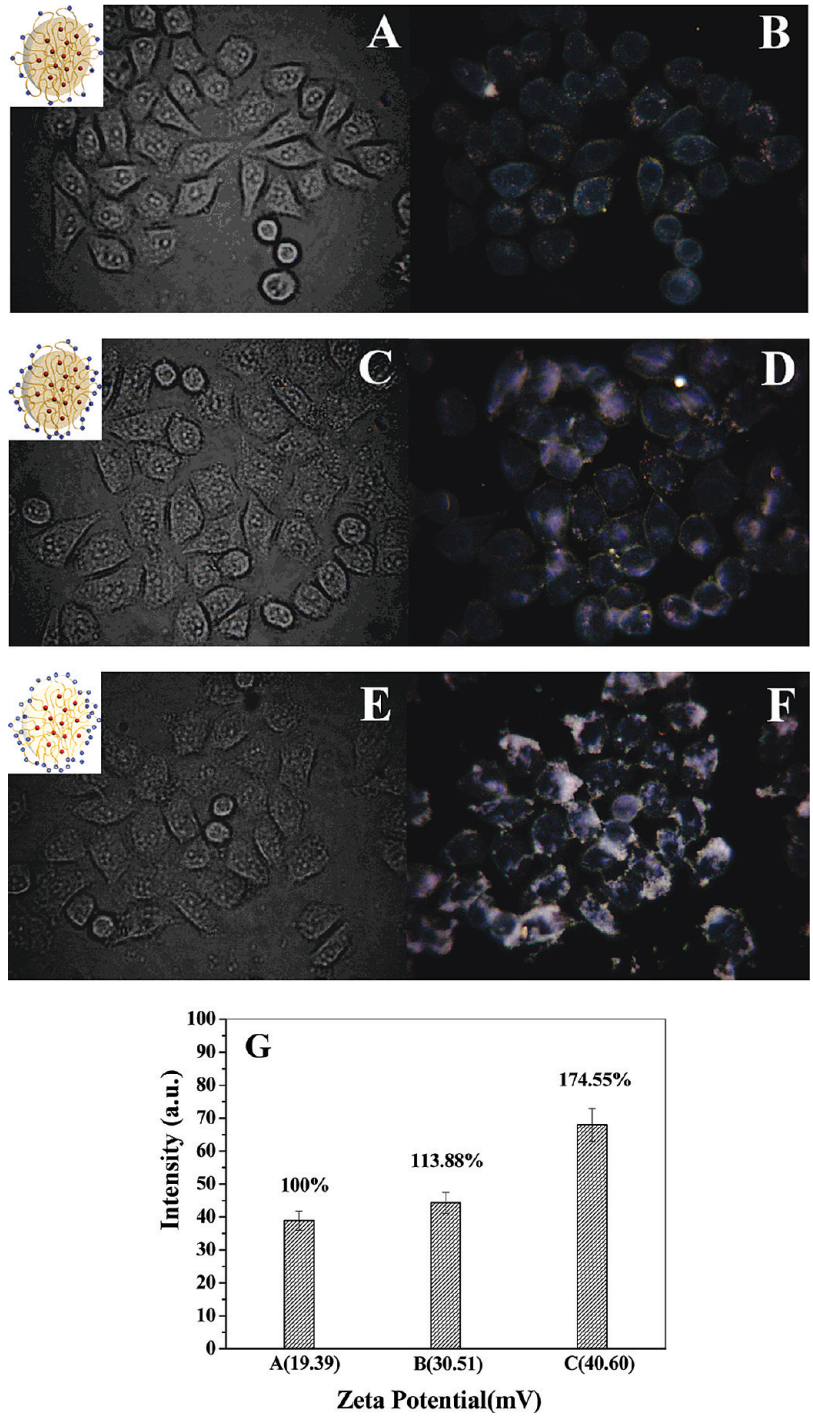

FIGURE 3. Uptake of CGHNs with varying surface potentials by BGC 823 cells. (A, C, E) Bright-field and (B, D, F) dark-field microscopic images of BGC 823 cells incubated with CGHNs for 4 h; surface zeta potentials of CGHNs are (A, B) 19.39, (C, D) 30.51, and (E, F) 40.60 mV; (G) relative amount of CGHN uptake by the cells using IPP software. Mean ± SD, $n = 4$; 40× objective. The concentration of CGHNs (chitosan-based) is 0.4 mg/mL culture medium.

mV, are all internalized into cells and lighten up the cells. Furthermore, a high dependence of surface zeta potential of CGHNs on the cell uptake is qualitatively observed by the brightness in the cells: the higher zeta potential, the better cell uptake. The semiquantitative analysis based on light-scattering intensity shown in Figure 3G and Figure S3 in the Supporting Information suggests that the cell uptake magnitude of CGHNs with varying surface potentials is in the order 40.60 > 30.51 > 19.39 mV. Semiquantitatively, the uptake of CGHNs with zeta potential of 40.60 and 30.51 mV by BG823 cells is 1.74 and 1.14 folds higher than that of CGHNs with zeta potential of 19.39 mV, respectively. The intracellular localization of CGHNs was also examined through dark-field images by virtue of the strong light scattering of gold particles. It can be seen that the disorder bright pink spots are inside BGC 823 cells for the sample with zeta potential of 19.39 mV (Figure 3B). Additionally, these CGHNs mainly accumulate in the cytoplasm of the cells, and do not penetrate into the nucleus. When the CGHNs with zeta potential of 30.51 mV were incubated with the BGC823 cells,

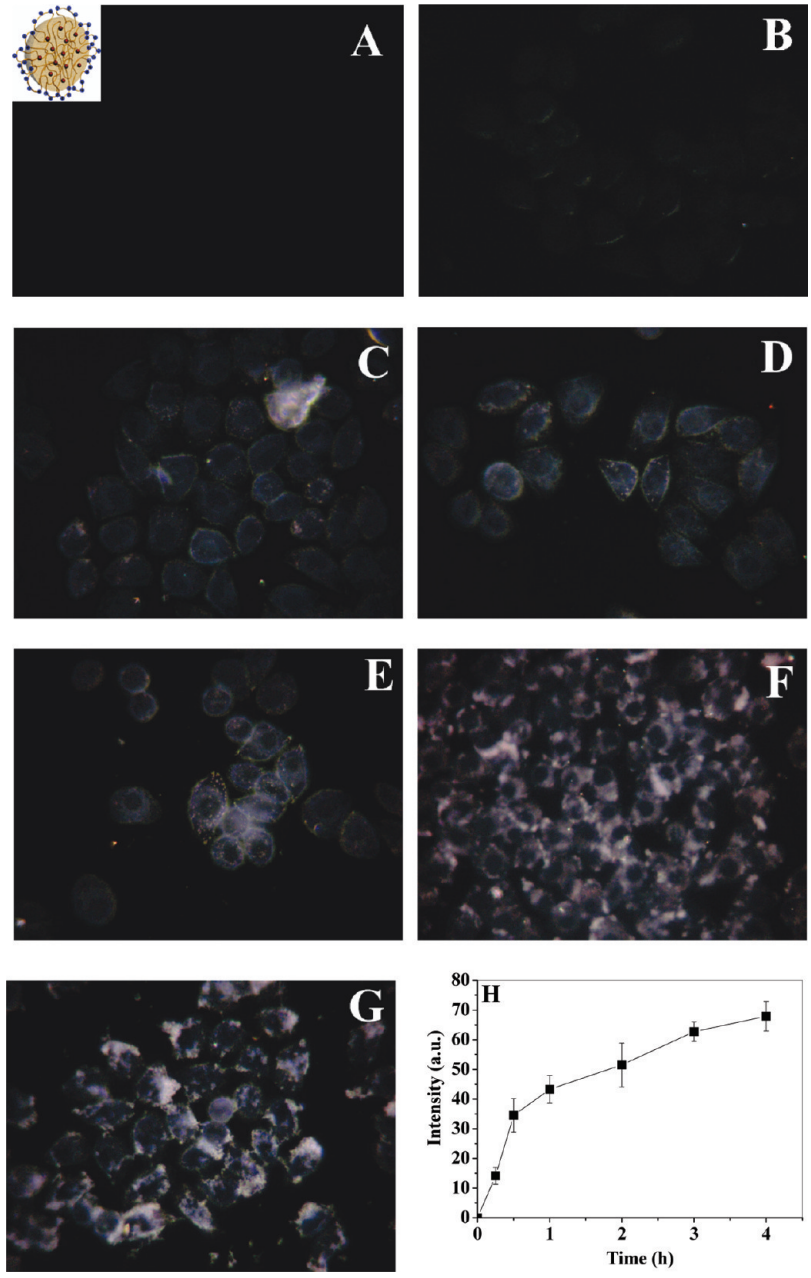

FIGURE 4. Dark-field images of BGC 823 cells coincubated with CGHNs with 40 mV zeta potential at different times. (A) 0 min, (B) 15 min, (C) 30 min, (D) 1 h, (E) 2 h, (F) 3 h, (G) 4 h. (H) Light-scattering intensity of cell coincubated with CGHNs with 40 mV zeta potential via incubation time; 40× objective. The concentration of CGHNs (chitosan-based) is 0.4 mg/mL culture medium.

there are more bright spots inside the cells with stronger brightness than that of CGHNs with 19.39 mV potential. Continually increasing the surface zeta potential of CGHNs to 40.60 mV produces stronger scattering light intensity from the cells. It is also found that no matter of the zeta potential magnitude of hybrid nanospheres, all dark-field images show punctate staining inside the cells, suggesting that the cell internalization of hybrid nanospheres follows the endosomal uptake, a signature for endocytosis uptake mechanism (25). These results indicate that the cell uptake of CGHNs is highly surface charge dependent and the cells prefer the particles with higher surface charge. However, some cellular membranes of BGC 823 cells in Figure 3F are incomplete, indicating highly positive-charged CGHNs would induce cellular membrane disruption/poration to enter cells, a process associated with cytotoxicity (25).

Kinetic Cell Uptake of CGHNs. To gain more complete understanding of particle internalization course and intracellular localization, we carried out further observing cellular uptake of CGHNs, using dark field microscopy, by cell internalization of high surface zeta potential CGHNs (40 mV) with varying incubation time: 0 min, 15 min, 30 min, 1 h, 2 h, 3 h, and 4 h, respectively (Figure 4A–G). It is clearly shown that there is no notable light scattering from CGHNs in the cells at the beginning of the incubation (Figure 4A). After theat, a continual increase in light scattering from the cells is seen with the incubation time (Figure 4B–G). At an incubation time of 15 min, only a few cell profiles can be

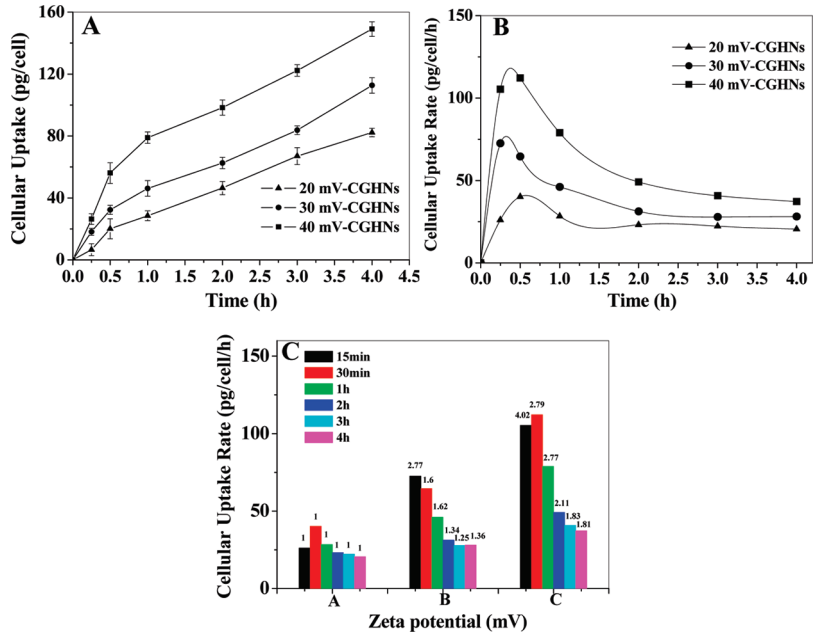

FIGURE 5. (A) Cell uptake quantity and (B, C) uptake rate of CGHNs by BGC 823 cells after 15 min, 30 min, 1 h, 2 h, 3 h, and 4 h incubation at 37 °C as a function of particle surface zeta potential (A = CGHNs with 20 mV, B = 30 mV and C = 40 mV). The concentration of CGHNs (chitosan-based) is 0.4 mg/mL culture medium.

distinguished (Figure 4B), indicating that a small amount of CGHNs is internalized into the cells within such a short time interval. Meanwhile, the whole cellular figure can be easily observed when the incubation time is extended to 30 min (Figure 4C). At this stage, it is found that most of the bright spots (scattering from the CGHNs) occupy the surface of cells or are close to the cell membrane inside the cells. This result suggests that at the beginning of the internalization process, particles may first adsorb onto the cellular surface by the interaction between positive-charged CGHNs and negatively charged cell membrane, and then the cell-surface-associated nanospheres are internalized into the cells by the endocytosis. With a further time extension, more and more CGHNs are internalized inside the cells, which not only lighten up the cell profile but also the cellular interior (Figure 4D–G). Particularly, with 4 h incubation, the CGHNs are located throughout the cells and some bright spots can be identified within the nucleus, indicating that chitosan nanospheres with high surface potential can enter the nucleus. To kinetically analyze the cell uptake of CGHNs, Image-Pro Plus (IPP) software was used to measure the light scattering intensity of the dark-field images corresponding to the different incubation time, and the light intensity via incubation time is plotted in Figure 4H. It can be seen that the scattering light intensity from the cells increases rapidly during the first 30 min, suggesting a fast absorption and uptake of the CGHNs by the cells. The increase rate in scattering light intensity then slows down, indicating that all binding sites at the membrane surface seem to be saturated by the CGHNs and newer binding sites are not yet available, which retards the cellular endocytic process.

The uptake of CGHNs with three different surface zeta potentials by BGC 823 cells exposed to CGHNs concentration of 0.4 mg/mL was also evaluated by measuring Au concentration in the cells with ICP-MS analysis. The time course of particle internalization was examined from 15 min to 4 h (Figure 5). Three kinds of the nanospheres all show an increase in cell uptake with the extending incubation time, and the total amount of Au content inside the cells within the same time course highly depends on the surface zeta potential of CGHNs (Figure 5A). The uptake rate of CGHNs by cells also depends on surface zeta potential of CGHNs, and all kinds of nanospheres have a maximum of uptake rate in the incubation time range of 20–30 min (Figure 5B). The cell uptake of CGHNs with 40.60 mV potential is 4.02- and 1.45-fold higher than that of ones with 19.39 and 30.51 mV potential at 15 min, respectively, but becomes 1.81- and 1.33-fold higher at 4 h (Figure 5C).

The uptake in BGC 823 cells was also examined by laser scanning confocal microscope (LSCM) using fluorescein isothiocyanate (FITC)-labeled CGHNs. Figure 6 shows the LSCM images of BGC 823 cells after incubation with FITC-labeled CGHNs with various zeta potentials for 4 h at 37 °C, in which the nuclei were selectively stained with Hoechst 33258 and show a blue color, whereas FITC-CGHNs show green color. From Figure 6A–C, it can be obtained that with increasing surface zeta potential of FITC-labeled CGHNs (from 19.39 to 40.60 mV), an increasing overlap of blue and green colors appears in the nuclear region, demonstrating again that higher positive surface potential can enhance the ability of CGHNs to enter cell nuclear.

In vitro Cytotoxicity of CGHNs. High-molecular-weight, positively charged polyelectrolytes such as polylysine and polyethylenimine are known to exhibit cytotoxicity in vitro because strong interactions between the polyelectrolytes and cell membrane phospholipids result in disruption of the cellular membrane structure (26, 27). To evaluate the cytotoxicity of CGHNs in vitro, cell viability on the CGHNs with various surface zeta potentials was examined by MTT

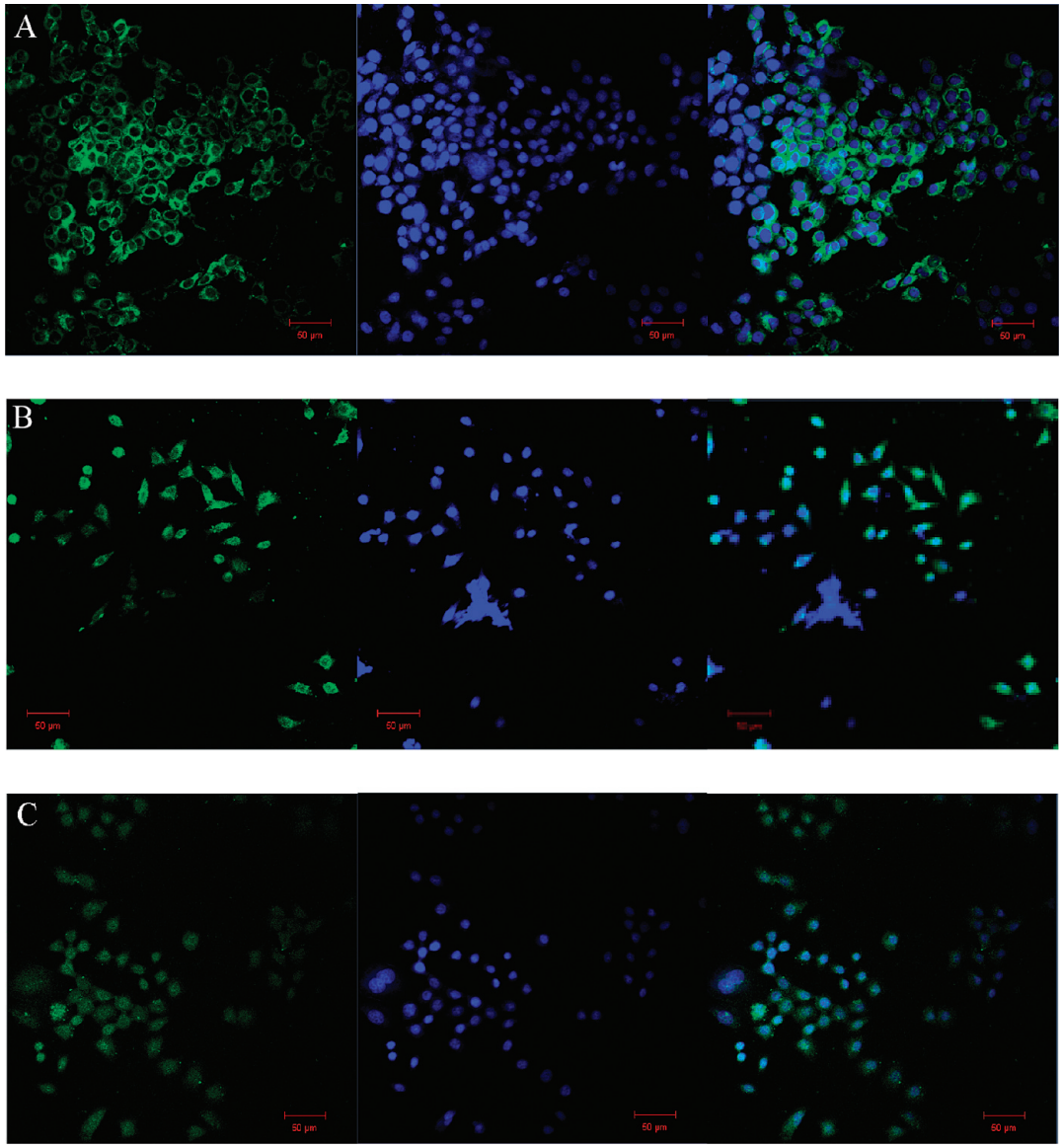

FIGURE 6. Confocal images of BGC 823 cells coincubated with FITC-labeled CGHNs with different surface zeta potentials. The nuclei were selectively stained with Hoechst 33258. (A = CGHNs with 20 mV, B = 30 mV, and C = 40 mV). Scale bars are 50 μm. The concentration of CGHNs (chitosan-based) is 0.4 mg/mL culture medium.

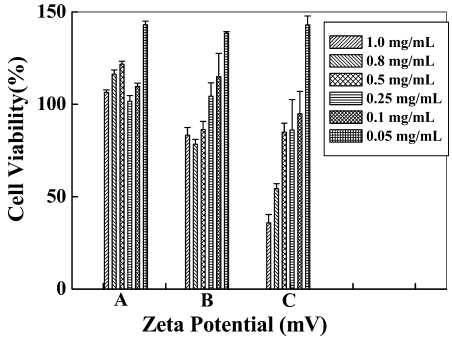

FIGURE 7. In vitro cytotoxicity of CGHNs with different surface zeta potential. (A = CGHNs with 20 mV, B = 30 mV, and C = 40 mV)

assay (Figure 7). The results suggest that CGHNs with 19.39 and 30.51 mV surface potentials show little cytotoxicity and cell proliferation is not hindered by CGHNs up to a concentration of 1.00 mg/mL in final cell culture medium. Although CGHNs with 40.60 mV surface potential show a concentration-dependent cytotoxic effect against BGC 823 cells and exhibit high cytotoxicity at the concentration higher than 0.8 mg/mL in final cell culture medium, yielding IC_{50} (IC_{50} represents the concentration at which 50% of cell growth were inhibited), about 0.8 mg/mL. This result indicates that the cytotoxicity of cationic CGHNs is directly related to their surface charge density. Since the ability of CGHNs to enter the cell and nucleus is also proportional to their surface positive charge density, the balance between their transmembrane crossing ability and cytotoxicity becomes very important in the rational design of polymer nanocarriers.

Intracellular Location of CGHNs. To track the spatial distribution of CGHNs inside the cells, TEM was used due to its high resolution. Figure 8 shows TEM images of BGC 823 cells after incubated with CGHNs (1.0 mg/mL) with various surface zeta potentials at 37 °C for 4 h. All these images verify that surface zeta potential of CGHNs does have

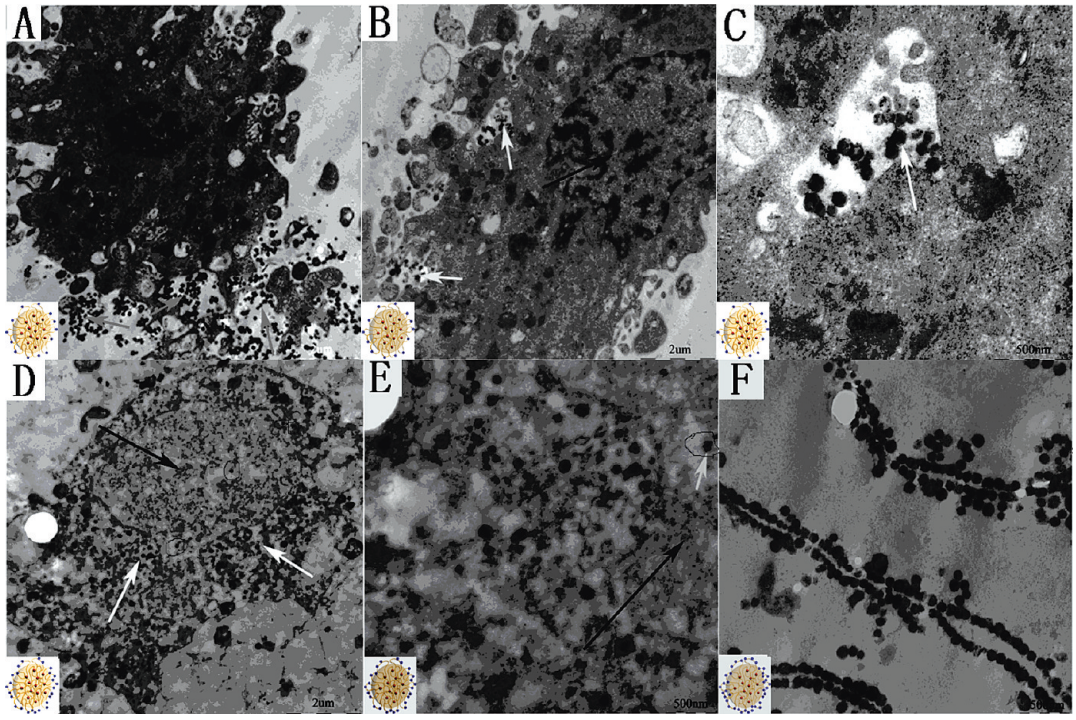

FIGURE 8. TEM images of BGC 823 cells incubated with CGHNs with different surface zeta potentials for 4 h at 37 °C: (A, B) 20 mV, (C) high magnification of B, (D) 30 mV, (E) high magnification of D, and (F) 40 mV. All slices were treated with uranyl acetate to stain membranes and lead citrate to stain the nuclear body. Arrows represent selected regions: nuclei (black) and CGHNs (white). The concentration of CGHNs (chitosan-based) is 1.0 mg/mL culture medium.

great influence on the cell uptake, intracellular location, and fate of CGHNs. Figure 8A–C shows the intracellular location of CGHNs with a 19.39 mV potential in BGC 823 cells. It follows that many CGHNs aggregates and huge vesicles, created by endocytosis process (28), are within the cell cytoplasm. With increasing surface potential of the CGHNs to 30.51 mV, it is found that most of CGHNs freely disperse in the cytoplasm (Figure 8D, E). Moreover, some CGHNs are found to be located in the nucleus. Additionally, vesicles loaded with CGHNs, as shown in images A and B in Figure 8, are not observed in this case. This result indicates that CGHNs with 30.51 mV surface potential have passed the vesicles transfer period and escaped from endosomal to the cytosol and even nucleus regions. In this sense, nucleus targeting can be enhanced by rationally increasing particle surface zeta potential. Further increasing surface potential to 40.60 mV, CGHNs exhibit a much high cytotoxicity, and almost no plasma membrane integrity can be observed in the TEM examination. Instead, CGHNs with 40.60 mV surface potential assemble into the lines (containing pieces of lipid bilayer as previous reports (29)) inside the cells, as shown in Figure 8F. This further confirms the cytotoxicity of CGHNs induced by higher surface charge density.

CONCLUSION

Organic fluorophore molecular have been widely used as imaging marks for the detection of trace levels of analytes. However, the photosensitivity of the fluorophores limits their application in complex environments, such as living biosystems where degradation or photobleaching can occur. In this paper, the potential of inorganic nanoparticles, such as gold nanoparticles, has been studied as a possible solution to this problem. Chitosan–gold hybrid nanospheres with varying surface zeta potentials were prepared to investigate cell internalization of chitosan nanospheres. We demonstrated that the surface potential of polymer nanospheres had significant biological implications in the transmembrane efficiency, intracellular fate and cytotoxicity of the nanospheres. The polymer nanospheres with higher surface potential had a faster cell uptake and a higher cell nuclear targeting ability as opposed to those with lower one. But a too high surface potential may destabilize the cell membrane and induce cell damage as well as cytotoxicity. Thus, the rational consideration of transmembrane crossing ability, surface charge density, and cytotoxicity for polymer nanopsheres will help us optimize the polymeric drug and gene nanocarriers.

Acknowledgment. This work was supported by the Natural Science Foundation of China (50625311 and 20874042) and the Cultivation Fund of the Key Scientific and Technical Innovation Project, Ministry of Education of China (707028).

Supporting Information Available: X-ray diffraction data for chitosan and chitosan–gold nanospheres; TEM images of hybrid nanospheres; light-scattering intensity of cells coincubated with hybrid nanoparticles (PDF). This material is available free of charge via the Internet at http://pubs.acs.org.

REFERENCES AND NOTES

(1) (a) Kim, D. K.; Park, S. J.; Lee, J. H.; Jeong, Y. Y.; Jon, S. Y. *J. Am. Chem. Soc.* **2007**, *129*, 7661–7665. (b) Ding, Y.; Hu, Y.; Jiang, X.; Zhang, L.; Yang, C. *Angew. Chem., Int. Ed.* **2004**, *43*, 6369–6372.

(2) Yang, J.; Lee, C. H.; Ko, H. J.; Suh, J. S.; Yoon, H. G.; Lee, K. Y.; Huh, Y. M.; Haam, S. J. *Angew. Chem., Int. Ed.* **2007**, *46*, 8836–8839.
(3) (a) Kang, Y. J.; Taton, T. A. *Angew. Chem., Int. Ed.* **2005**, *44*, 409–412. (b) Lee, H.; Lee, E.; Kim, D. K.; Jang, N. K.; Jeong, Y. Y.; Jon, S. Y. *J. Am. Chem. Soc.* **2006**, *128*, 7383–7389.
(4) Wolinsky, J. B.; Grinstaff, M. W. *Adv. Drug Delivery Rev.* **2008**, *60*, 1037–1055.
(5) Zhang, G. D.; Harada, A.; Nishiyama, N.; Jiang, D. L.; Koyama, H.; Aida, T.; Kataoka, K. *J. Controlled Release* **2003**, *93*, 141–150.
(6) Gref, R.; Minamitake, Y.; Peracchia, M. T.; Trubetskoy, V.; Torchilin, V.; Langer, R. *Science* **1994**, *263*, 1600–1603.
(7) Roy, K.; Mao, H. Q.; Huang, S. K.; Leong, K. W. *Nat. Med.* **1999**, *5*, 387–391.
(8) Williams, D. F. *Definitions in Biomaterials: Proceedings of a Consensus Conference of the European Society for Materials*; Chester, U.K., March 3−5, 1986; Williams, D. F., Ed.; Elsevier: Amsterdam, 1987.
(9) Allen, T. M.; Cullis, P. R. *Science* **2004**, *303*, 1818–1822.
(10) (a) Choleris, E.; Little, S. R.; Mong, J. A.; Puram, S. V.; Langer, R.; Pfaff, D. W. *Proc. Natl Acad. Sci. U.S.A.* **2007**, *104*, 4670–4675. (b) Chithrani, B. D.; Chan, W. C. W. *Nano Lett.* **2007**, *7*, 1542–1550. (c) Chithrani, B. D.; Ghazani, A. A.; Chan, W. C. W. *Nano Lett.* **2006**, *6*, 662–668.
(11) (a) McNeil, S. E. *J. Leukocyte Biol.* **2005**, *78*, 585–594. (b) Oh, J. M.; Choi, S. J.; Kim, S. T.; Choy, J. H. *Bioconjugate Chem.* **2006**, *17*, 1411–1417. (c) Huang, D. M.; Hung, Y.; Ko, B. S.; Hsu, S. C.; Chen, W. H.; Chien, C. L.; Tsai, C. P.; Kuo, C. T.; Kang, J. C.; Yang, C. S.; Mou, C. Y.; Chen, Y. C. *FASEB J.* **2005**, *19*, 2014–2038. (d) Ma, Z.; Lim, L. Y. *Pharm. Res.* **2003**, *20*, 1812–1819. (e) Huang, M.; Ma, Z.; Khor, E.; Lim, L. Y. *Pharm. Res.* **2002**, *19*, 1488–1494.
(12) (a) Mansouri, S.; Cuie, Y.; Winnik, F.; Shi, Q.; Lavigne, P.; Benderdour, M.; Beaumont, E.; Fernandes, J. C. *Biomaterials* **2006**, *27*, 2060–2065. (b) Davda, J.; Labhasetwar, V. *Int. J. Pharm.* **2002**, *233*, 51–59. (c) Sahoo, S. K.; Panyam, J.; Prabha, S.; Labhasetwar, V. *J. Controlled Release* **2002**, *82*, 105–114. (d) Chawla, J. S.; Amiji, M. M. *Int. J. Pharm.* **2002**, *249*, 127–138.
(13) Harush-Frenkel, O.; Debotton, N.; Benita, S.; Altschuler, Y. *Biochem. Biophys. Res. Commun.* **2007**, *353*, 26–32.
(14) Cho, E. C.; Xie, J. W.; Wurm, P. A.; Xia, Y. N. *Nano Lett.* **2009**, *9*, 1080–1084.
(15) Maysinger, D.; Lovrić, J.; Eisenberg, A.; Savić, R. *Eur. J. Pharm. Biopharm.* **2007**, *65*, 270–281.
(16) Delie, F. *Adv. Drug Delivery Rev.* **1998**, *34*, 221–233.
(17) Xu, C.; Xie, J.; Ho, D.; Wang, C.; Kohler, N.; Walsh, E. G.; Morgan, J. R.; Chin, Y. E.; Sun, S. *Angew. Chem., Int. Ed.* **2008**, *47*, 173–176.
(18) Tsai, S. W.; Chen, Y. Y.; Liaw, J. W. *Sensors* **2008**, *8*, 2306–2316.
(19) El-Sayed, H.; Huang, X. H.; El-Sayed, M. A. *Nano Lett.* **2005**, *5*, 829–834.
(20) Hu, Y.; Chen, Q.; Ding, Y.; Li, R. T.; Jiang, X. Q.; Liu, B. R. *Adv. Mater.* **2009**, *21*, 3639–3643.
(21) Guo, R.; Zhang, L. Y.; Zhu, Z. S.; Jiang, X. Q. *Langmuir* **2008**, *24*, 3459–3464.
(22) Moore, S. *J. Biol. Chem.* **1968**, *243*, 6281–6283.
(23) Yeh, P. Y.; Kopeckova, P.; Kopecek, J. *J. Polym. Sci., Part A: Polym. Chem.* **1994**, *32*, 1627–1637.
(24) Massa, T. M.; Yang, M. L.; Ho, J. Y. C.; Brash, J. L.; Santerre, J. P. *Biomaterials* **2005**, *26*, 7367–7376.
(25) Verma, A.; Uzun, O.; Hu, Y.; Hu, Y.; Han, H. S.; Watson, N.; Chen, S.; Irvine, D. J.; Stellacci, F. *Nat. Mater.* **2008**, *7*, 588–595.
(26) Garnett, M. C. *Crit. Rev. Ther. Drug Carrier Syst.* **1999**, *16*, 147–207.
(27) Zauner, W.; Ogris, M.; Wagner, E. *Adv. Drug Delivery Rev.* **1998**, *30*, 97–113.
(28) Möbius, W.; Donselaar, E. V.; Ohno-Iwashita, Y.; Shimada, Y.; Heijnen, H. F. G.; Slot, J. W.; Geuze, H. J. *Traffic* **2003**, *4*, 222–231.
(29) Taraska, J. W.; Almers, W. *Proc. Natl. Acad. Sci. U.S.A.* **2004**, *101*, 8780–8785.

AM1001019